Clays and Clay Minerals, Vol. 38, No. 2, 187–195, 1990.

FORMATION OF TRIOCTAHEDRAL ILLITE FROM BIOTITE IN A SOIL PROFILE OVER GRANITE GNEISS

A. W. FORDHAM

Division of Soils, CSIRO, Private Bag No. 2
Glen Osmond, 5064, South Australia, Australia

Abstract—Clay fractions separated from the A2, B, and C horizons of a soil formed on granite gneiss showed X-ray powder diffraction (XRD) spacings characteristic of trioctahedral illite. The trioctahedral illite was derived from biotite, and its development through various stages of weathering was followed by optical and electron microscopy combined with electron microanalysis. In the initial stages of weathering, Fe^{2+} within biotite was oxidized, without the loss of much K. During this process, biotite flakes became slightly buckled and fractured. Solutions moved into the damaged flakes leading to chemical weathering and exfoliation along cleavages and angular fractures. Major exfoliation broke up the flakes into segments, which themselves contained minor exfoliations and alterations along cleavage planes. The extent of exfoliation and alteration continued until thinner and shorter segments consisted almost wholly of thin (<0.25 μm), parallel wafers separated by less compact layers of particles and microaggregates. The segments finally lost their shape and divided into clay-size particles. Parts of the thin wafers had the same chemical composition (and structure) as the original, intact flakes of oxidized biotite. The same parts of wafers retained some of the optical properties of the original biotite, and, when broken down to clay, they produced the XRD spacings of 10 and 1.54 Å, typical of fine-grained, trioctahedral mica (illite).

Key Words—Biotite, Electron microprobe, Illite, Mica, Scanning electron microscopy, Trioctahedral, Weathering, X-ray powder diffraction.

INTRODUCTION

The definition of illite is not yet clearly established (Bailey *et al.*, 1971; Środoń and Eberl, 1984), but the name is used in this paper to mean a fine-grained mica (Norrish and Pickering, 1983). In its dioctahedral form, illite is common in soils throughout the world. On the other hand, trioctahedral illite is relatively rare. Walker (1950) recorded trioctahedral illite in clay fractions from a few relatively unweathered parent materials in Scotland. X-ray powder diffraction (XRD) showed strong, sharp, first-order basal reflections at 10 Å and medium to strong 060 reflections at 1.53 Å. In the upper parts of the profiles, exchange of K in the illite caused broadening of the 10-Å peak and the appearance of wide bands from 10 to 14 Å, which subsequently resolved into two diffuse peaks at 10 and 14 Å. The 10-Å peak eventually disappeared as the illite was converted completely to vermiculite. Wilson (1970) found trioctahedral illite in association with interstratified vermiculite chlorite, kaolinite, and gibbsite in the clay fractions of three Scottish soils. He described the illite as mechanically degraded cores of unweathered biotite remaining within weathered flakes.

Nettleton *et al.* (1973) reported that clay fractions of many soils in the southwestern United States, particularly from the surface horizons, contained clay minerals having 10-Å (and presumably 1.54-Å) spacings, derived from weathering of biotite. They concluded that trioctahedral illite was reconstituted by reaction of K from decaying plant residues with earlier weathering products of biotite, namely, interstratified biotite/vermiculite and vermiculite. Tarzi and Protz (1979) and Ghabru *et al.* (1987) supported this view. Kapoor (1972) described trioctahedral illite as a major component of clays in the lower horizons of many Scandinavian soils. There, it weathered to hydrobiotite in the surface horizons and subsequently to vermiculite, smectite, and interstratified smectite/chorite. Norrish and Pickering (1983) commented that trioctahedral illites are rare in Australian soils and are only found in young soils formed from rocks containing biotite or phlogopite. Chartres *et al.* (1988) recently reported trioctahedral mica in the clay fractions of four soil profiles developed on granitic rocks in southeastern Australia.

The relatively rare occurrences of trioctahedral illites in soil clays is due largely to the reactive nature of biotite itself. In most circumstances, biotite loses K quite rapidly and is then capable of interlayer expansion to form interstratified materials, vermiculite, and smectite. Ferrous iron in the structure is susceptible to oxidation and, according to most reports (Walker, 1949; Wilson, 1970; Seddoh and Pedro, 1974), oxidation takes place at an early stage of weathering. In biotites having a moderate to high amount of iron, this oxidation causes instability as excess charge builds up in the octahedral layer, and it results in the expulsion of Fe from the structure (Walker, 1949; Farmer *et al.*, 1971) and partial conversion from trioctahedral to dioctahedral character (Robert and Pedro, 1969; Farmer *et al.*, 1971;

Gilkes *et al.*, 1972). Paradoxically, biotite after oxidation and reestablishment of a more stable structure, then holds its K more tightly than before (Gilkes, 1973; Gilkes and Young, 1974; Ross and Rich, 1974), and oxidized vermiculites readsorb K strongly and selectively (Barshad and Kishk, 1968).

In the present study, trioctahedral illite and other weathering products of biotite were identified in soil clay fractions. The manner in which biotite altered to clay was followed by optical and scanning electron microscope observations on thin sections of soil and parent material. Microanalytical data from all stages of weathering were used to derive the probable chemical composition of the trioctahedral illite.

MATERIALS AND METHODS

Site and soil description

The samples were collected at Mt. Crawford, about 80 km northeast of Adelaide, South Australia. Full details are reported elsewhere (Fordham *et al.*, 1985), but a brief description is included here to indicate the environmental conditions. The climate at Mt. Crawford is mediterranean, with hot (27°C max, 11°C min), dry summers and mild (15°C max, 3°C min), wet winters. More than 70% of the annual rainfall of 770 mm occurs during the winter months. The site is near the top of a saddle only 20 m below the maximum elevation of 470 m in the immediate vicinity. Slope at the site is 3°–5° to the southeast. Mainly yellow podzolic (Stace *et al.*, 1968) or Palexeralf (Soil Survey Staff, 1975) soils have developed on parent material of granite gneiss, which locally is intruded by thin pegmatite dikes along joint planes. Boulders of granite gneiss are exposed at the surface at several places near the site, some within meters of one of the trenches from which samples were taken.

The soil profile contains an A horizon of sandy-loam texture which extends to 30–40 cm below the surface. The lower part is commonly bleached. A 5–10-cm-wide stone line of granite gneiss and quartz gravel exists at about 15 cm depth, and locally small (5–10 cm), partly weathered corestones of granite gneiss occur near the base of the horizon. Below the A horizon is a B horizon of medium-heavy clay texture, usually from 5 to 20 cm thick. It merges into a clay band as wide as 10 cm, which forms the weathering rind enclosing subsurface core boulders of granite gneiss about 1 m in diameter. In places, both the B horizon material and the weathering rind are absent, so that the A horizon is in direct contact with the subsurface boulders.

Soils formed over pegmatite have A horizons of sandy loam texture similar to that over granite gneiss. The stone line of quartz and granite gneiss gravel is absent, but, in its place, there is a layer of very coarse feldspar and quartz fragments which merges into consolidated pegmatite.

Analytical methods

The method of preparing thin sections and the techniques of microanalysis were described by Fordham (1990). Clay fractions were prepared for XRD by mixing samples mechanically in 1.0 M NaCl solutions and treating them ultrasonically before fractionating them by the usual techniques of sedimentation and centrifugation. No other chemical pretreatments were used.

Samples of biotite were obtained for XRD and chemical analysis from both exposed and subsurface boulders. The rock was crushed as gently as possible and larger hand-picked flakes were added to smaller ones recovered by sifting on slightly rough paper (Wilson, 1966). The material so obtained was ground lightly and biotite was again collected, this time with a very strong bar magnet. The most highly magnetic particles, obtained by passing the magnet close to but not touching the surface of the spread-out sample, were discarded. Chemical analysis of the separated biotites was made after digestion of 1-g samples in hydrofluoric and sulfuric acids. Total Fe was measured by atomic absorption spectrometry, and Fe(II) was measured by titration against potassium dichromate.

XRD patterns were recorded with a Philips PW1710 microprocessor-controlled diffractometer using CoKα radiation, variable divergence slits, and a graphite monochromator. Scanning electron microscope (SEM) observations were made in a Cambridge Stereoscan Mk.250, fitted with a Link energy-dispersive X-ray (EDX) detector. Colors seen in the petrological microscope were defined according to the Munsell system.

RESULTS AND DISCUSSION

XRD evidence for the presence of trioctahedral illite

XRD patterns of untreated random powder mounts are shown in Figure 1. They include tracings of hand-picked biotite flakes from both exposed and subsurface boulders, together with clay fractions separated from samples taken from the weathered rind about a subsurface boulder, from a thin clay band below one and above another subsurface boulder, from the lower part of the B horizon, and from the A2 horizon.

At high 2θ values, at which the distinction between trioctahedral and dioctahedral micas is usually made from the position of the 060 reflection, fresh biotite from exposed boulders shows a narrow peak extending from 1.547 to 1.542 Å. According to XRD data tabulated by Bailey (1984), this peak could contain contributions from other reflections, such as $33\bar{1}$, $20\bar{6}$ and 135, as well as 060. Biotite from the interior of subsurface boulders, which contains substantially more oxidized Fe than biotite from exposed boulders (see below), shows sharp, overlapping peaks at 1.540 and 1.535 Å. Quartz, which has a peak at 1.541 Å, is absent. At the next stage of weathering, namely, in the <2-μm

https://doi.org/10.1346/CCMN.1990.0380210 Published online by Cambridge University Press

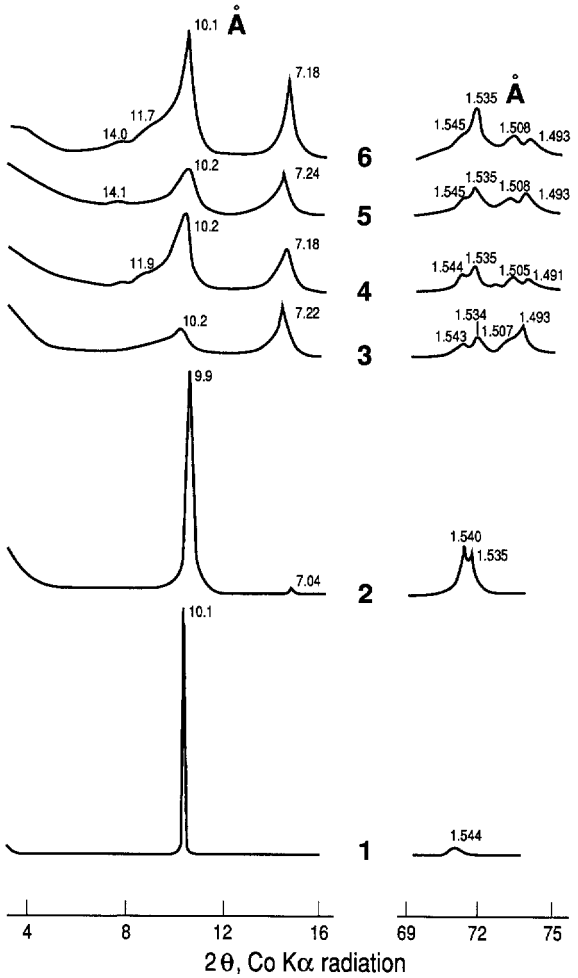

Figure 1. Smoothed X-ray powder diffraction patterns of untreated random powders: 1, Fresh biotite flakes from an exposed boulder; 2, Biotite flakes from interior of a subsurface boulder; 3, <2.0-μm clay fraction from weathering rind about a subsurface boulder; 4, 0.2–2.0-μm clay fraction from clay band between subsurface boulders; 5, 0.2–2.0 μm clay fraction from lower B horizon; 6, 0.2–2.0-μm clay fraction from A2 horizon.

clay fraction from the rind of a subsurface boulder, the peak at 1.534 Å has a greater intensity that at 1.543 Å, and additional peaks at 1.507 Å and 1.493 Å are present. The peak at 1.507 Å is due to dioctahedral illite formed from muscovite and perhaps biotite, and the peak at 1.493 Å is due to kaolinite. In the 0.2–2.0-μm clay fractions from other more weathered parts of the soil profile, the 1.535 Å peak is more intense than the peak near 1.54 Å, which occurs as a broad shoulder.

According to several workers, including Gilkes *et al.* (1972) and Gilkes and Suddhiprakarn (1979), the *b*-axis spacing of biotite decreases with increasing degree of oxidation of structural Fe. This relationship is consistent with the present work, as seen by comparing

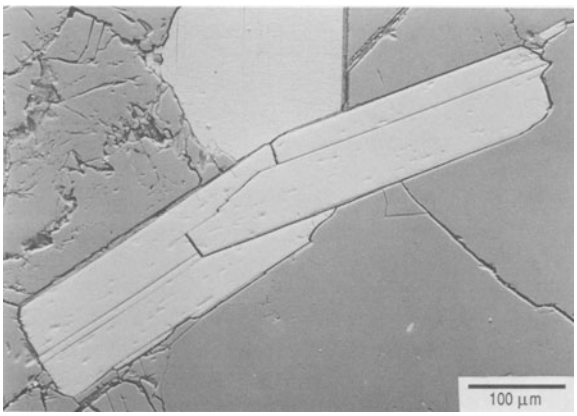

Figure 2. Secondary electron image of unweathered, partially oxidized biotite in thin section from exposed boulder.

peaks in fresh biotite from exposed boulders with those of samples from within the profile. The 060 peaks of the artificially oxidized biotites of Gilkes *et al.* (1972) decreased from 1.542 to 1.533 Å as the Fe^{3+} content increased from 18% to 77% of total Fe content. The decrease of *b*-axis dimension was attributed to the smaller ionic size of Fe^{3+} relative to Fe^{2+}, and also to the possible expulsion of octahedral cations in response to the increased charge.

At low 2θ values, the 10-Å peak of fresh biotite from exposed boulders is sharp and intense. The corresponding peak of biotite from the interior of subsurface boulders is slightly broader, particularly on the low angle side, and a small peak at 7 Å is probably due to the presence of kaolinite. As noted also by Gilkes and Suddhiprakarn (1979), the 7-Å peak is displaced to higher d-values as weathering increased. In these more weathered samples, the 10-Å peaks are much broader on the low-angle side, and some show small shoulders at about 12 and 14 Å. These effects will be discussed in more detail elsewhere.

Changes in the appearance of biotite during weathering

Hand specimens of biotite from exposed boulders had a fresh, shiny appearance and were black with a greenish tinge. In thin sections the crystals showed a euhedral rectangular shape (Figure 2), about 0.2 mm wide and 0.5 to 2.0 mm long. Apart from a few enclosed slits in which cleavage planes had opened slightly, no obvious physical signs of decomposition were noted.

Biotite from the interior of subsurface boulders was also fresh, shiny and black to the naked eye, but it lacked the greenish tinge, and some flakes had a golden sheen in strong reflected light. The interior of the rock itself was not stained. In thin section, clear evidence of alteration was found: transverse sections of the least weathered flakes still had a rectangular shape, but many were slightly curved lengthwise, and the edges were

https://doi.org/10.1346/CCMN.1990.0380210 Published online by Cambridge University Press

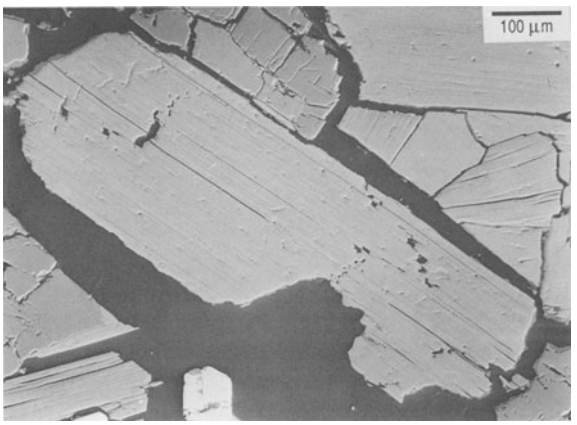

Figure 3. Secondary electron image of oxidized biotite in thin section from the interior of a subsurface boulder.

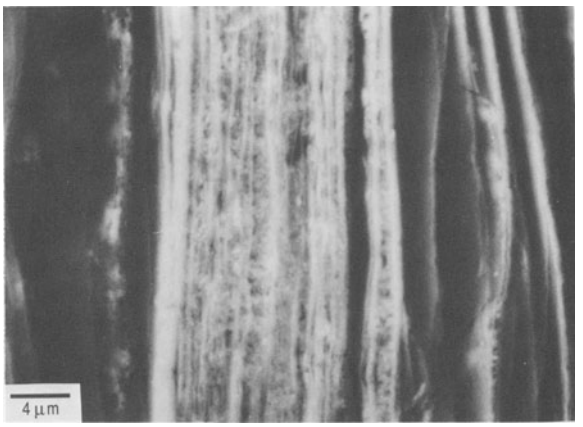

Figure 4. Backscattered electron image of fine exfoliations and deposits in thin section from the rind of a subsurface boulder.

eroded and frayed (Figure 3). Internal slits were more common and more extensive, although they rarely extended completely across a flake. Very fine fractures were present, transecting the breadth of the flakes in a jagged, angular fashion, roughly at right angles to the cleavage planes and commonly near the edges. Similar fine fractures in biotite were observed by Bisdom (1967) and larger fractures by Ghabru *et al.* (1987). Small erosion pits were noted in the body of the flakes, some perhaps where heavy mineral inclusions originally existed in the unweathered mineral, as suggested by Tarzi and Protz (1978) and Shoba and Sokolova (1981). Further evidence of buckling and distortion was given by curved and sometimes concentric cleavage lines which were noted in some basal sections. Although several samples from different subsurface boulders were examined, unweathered biotite similar to biotite from exposed boulders was not found.

The next phase of weathering was best observed in the weathered rind around subsurface boulders. In thin section, the slits within biotite flakes were no longer enclosed, but extended the whole length of the flakes. As weathering progressed, such exfoliations became wider and more numerous and divided the flake into segments, commonly having splayed ends. Biotite at this stage of weathering was described thoroughly by Bisdom (1967), Bustin and Mathews (1979), Gilkes and Suddhiprakarn (1979), Penven *et al.* (1981), and Bisdom *et al.* (1982). What is not obvious or what was not emphasized in these publications is that the segments themselves contained much finer exfoliations parallel to the cleavage and usually filled with decomposition products (seen in Figure 4). The flakes remained intact if segments were held together by individual strands acting like a flat spring, namely, each strand stretched across wider exfoliations and had either end attached to the upper and lower segments.

As the restraining skeleton of the rock fabric was lost and individual particles became subject to additional stress and turbulence, as in the B horizon, segments between exfoliations became dislocated and behaved subsequently as separate entities or locally took on the distorted appearance shown in Figure 5. The B horizon contained a range of weathering stages from moderately to extensively exfoliated but still intact flakes to isolated segments (usually disoriented with respect to each other but still localized in groups, indicating a common origin), becoming thinner and shorter with further decomposition. The finely stranded nature of the segments became exaggerated with increased weathering (Figure 6).

In the A2 horizon and in parts of the upper B horizon immediately adjacent to the A2, only a few large flakes of weathered biotite were noted (Figure 7). These appeared to have survived the most intense weathering

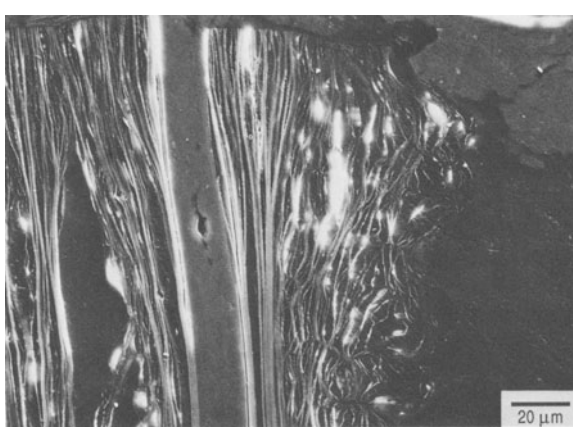

Figure 5. Backscattered electron image of distorted and dismembered strands of weathered biotite in thin section from B horizon. Wide exfoliation in the center is packed with transported clay.

https://doi.org/10.1346/CCMN.1990.0380210 Published online by Cambridge University Press

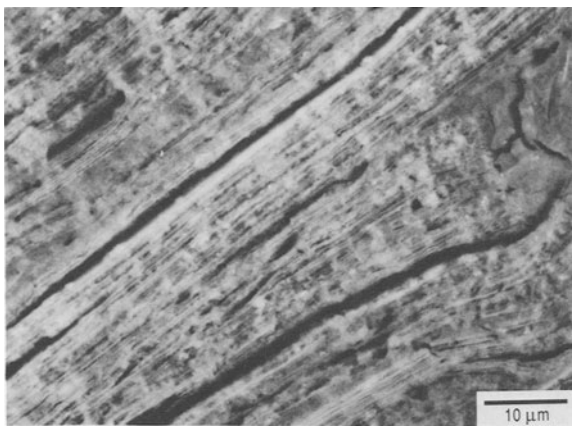

Figure 6. Backscattered electron image of finely exfoliated lath in thin section from B horizon.

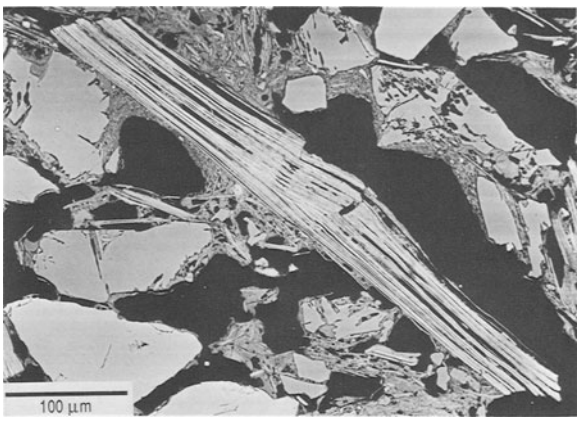

Figure 7. Backscattered electron image of a relatively large fragment of weathered biotite in thin section from A2 horizon.

processes, and, although extensively exfoliated, they contained relatively wide strands of apparently unweathered material. Apart from these flakes, biotite occurred most frequently as small, thin segments, usually about 20 μm in length (also seen in Figure 7). These segments also contained fine exfoliations in the cleavage direction and had a whispy appearance in the optical microscope.

Oxidation state of iron in biotite

Chemical analysis of fresh biotite from exposed boulders shows that it contains 18.5% FeO and 13.9% Fe_2O_3, that is, 60% of the total Fe is ferrous and 40% is ferric. By contrast, the corresponding values for biotite from the interior of subsurface boulders are 1.7% FeO and 21.5% Fe_2O_3, indicating that even the least weathered biotite in the soil profile (including the parent material) already had 93% of its total Fe in the oxidized form.

This difference in the oxidation state of Fe at the two locations was reflected in the color of biotite in thin sections. Viewed in a petrological microscope, transverse sections of biotite from exposed boulders were pleochroic, changing from pale olive (5Y 6/4) to dark olive gray (5Y 3/2). Between crossed polars, they were uniformly olive (5Y 5/4), as interference colors were superimposed on the color of the mineral. In contrast, the color change in flakes from the interior of subsurface boulders (and elsewhere in the profile where the flakes were not too extensively weathered) was from yellow (2.5Y 7/6) to yellow-brown (10YR 5/6), whereas between crossed polars, the flakes showed distinct second-order interference colors, with green predominating over yellow and orange. Even the most weathered segments, for example, those in the B horizon, commonly retained traces of second-order green.

Although the color of biotite is not an unequivocal guide to the oxidation state of structural iron (see Rossman, 1984), it can be accepted with confidence here because the comparison has been made between samples of similar chemical composition. Consequently, all the Fe measured by microprobe in weathered biotite is expressed as Fe_2O_3 in the following sections, unless otherwise stated.

Microprobe analyses in thin section

Electron microprobe analyses of fresh biotite in thin sections of exposed boulders produced a consistent set of results having low variability. The average data are recorded in Table 1, with total Fe partitioned between FeO and Fe_2O_3 in accordance with the Fe^{2+}/Fe^{3+} ratio measured by chemical analysis of biotite from the same source. Total Fe contents by microprobe agree well with those by chemical analysis (see above). The ratio of Fe^{2+} to Fe^{3+} in fresh biotite is relatively low compared with those of many samples tabulated by Deer *et al.* (1962), which suggests some oxidation may have already taken place.

As discussed by Fordham (1989), point analyses by microprobe are difficult to decipher unless a relatively pure mineral phase has been analyzed. Once weathering began in the biotite system, such phases became increasingly rare, but a few were encountered, as in the two examples described below.

1. Transverse sections of biotite flakes from the interior of subsurface boulders contained substantial unblemished areas, i.e., they appeared to be free of slits, erosion pits, inclusions, or other defects when viewed at high magnification in the backscatter mode of the SEM. Data measured in these areas are given in Table 1, with, as before, the total Fe distributed between FeO and Fe_2O_3 according to the appropriate chemical analysis. As can be seen by the small standard deviations, these points represent a relatively homogeneous composition, even though they were measured in several different flakes. This material was the least

https://doi.org/10.1346/CCMN.1990.0380210 Published online by Cambridge University Press

Table 1. Measured (electron microprobe) and estimated chemical compositions (wt. %) of weathered biotite.[1]

Description	SiO_2	Al_2O_3	TiO_2	FeO	Fe_2O_3	MgO	K_2O	Na_2O	CaO	Total	Si/Al
Fresh biotite	32.8	15.3	3.4	18.9	14.1	3.2	9.2	0.2	0.0	97.1	1.89
Standard deviations (9 points)	(0.5)	(0.3)	(0.2)	(0.3)	(0.3)	(0.2)	(0.1)	(0.1)	(0.0)	(0.5)	(0.02)
Unblemished areas[2]	35.3	15.7	2.3	1.7	22.4	7.7	8.7	0.1	0.0	93.9	1.98
Standard deviations (11 points)	(0.9)	(0.2)	(0.1)	(0.1)	(0.9)	(0.3)	(0.2)	(0.0)	(0.0)	(1.0)	(0.04)
Fragments in A2 horizon[2]	34.5	15.8	2.5	1.8	23.0	7.3	8.1	0.2	0.1	93.3	1.91
Standard deviations (12 points)	(1.9)	(0.6)	(0.2)	(0.2)	(2.5)	(0.9)	(0.5)	(0.1)	(0.0)	(2.1)	(0.04)
Oxidized biotite	34.4	14.8	2.9	1.7	22.1	8.7	9.2	0.2	0.0	94.0	2.05

[1] Total Fe and FeO measured by atomic absorption and by titration against potassium dichromate, respectively.
[2] See text.

weathered biotite encountered in the subsurface boulders.

2. Fragments of weathered biotite remaining in the A2 horizon contained many exfoliations, both large and small. Many of the microprobe analyses of strands between visible exfoliations indicate the presence of decomposition products presumably within even finer, undetected exfoliations. A few such strands, however, appeared to have been relatively uncontaminated, or else decomposition products had been removed by leaching. Analyses at such points are given in Table 1. Allowing for the fact that these analyses probably include some contribution from decomposition products, the material here is essentially the same as that in unblemished areas of flakes from the interior of subsurface boulders. This implies that oxidized biotite had a reasonable degree of stability if it was displaced from regions of more intense weathering, such as existed in deeper parts of the profile. In the deeper parts, for example, in the weathering rind of subsurface boulders, in clay bands between subsurface boulders, or in the lower B horizon, decomposition has progressed to produce such fine-scale alteration, that the microprobe was not able to discriminate between phases.

Oxidized biotite and trioctahedral illite

The microprobe data for unblemished areas and for A2 fragments, after being processed and plotted on a graph of K_2O content vs. Si/Al ratio, as described by Fordham (1989), give points close to the apex of oxidized biotite. This component is one of three (apart from free iron oxides) in the biotite system that can be mixed in appropriate proportions to give an analytical composition matching that of any of the microprobe analyses made of biotite in all stages of weathering. As biotite deteriorated into finely exfoliated segments, the wider strands usually were found to contain a high proportion of oxidized biotite. Even after weathering had progressed to the stage where the wider strands subdivided again and again to produce very fine, closely-set strands (or wafers, in three dimensions) separated by equally narrow layers containing particulate material, oxidized biotite was still present at least as a minor component in the volume of material analyzed by microprobe (about 5 μm^3). At some points, oxidized biotite was identified as a separate phase; in others, it formed layers within interstratified minerals (to be described elsewhere).

Many of the microprobe analyses showing contributions from oxidized biotite were undoubtedly obtained from clay-size material. In addition, somewhat larger, strongly weathered fragments containing oxidized biotite probably broke down during laboratory preparation of the clay fractions. Consequently, the XRD characteristics of fine-grained mica or trioctahedral illite observed in the clay fractions are attributed to oxidized biotite, and the chemical composition derived from microprobe analyses for oxidized biotite in all size of particles (Table 1) may also be applied to clay-size trioctahedral illite.

Status of iron in oxidized biotite or trioctahedral illite

One of the most difficult aspects of studying biotite weathering is to define whether all or only some of the Fe measured in weathered particles is an integral part of the biotite crystal structure. Free iron oxides are certainly deposited in exfoliations or otherwise in close association with biotite during early stages of its alteration to clay minerals; however, because the iron oxides are usually in such a fine state, they are not recognizable in the SEM until they are present in excess or accumulated into microaggregates. All the data used in Figure 7 of Fordham (1989) were measured at points within the framework of recognizable remnants of weathered biotite. Many showed the presence of excess iron oxides by their strong coloring, but not all. By plotting the raw data used in Figure 7 as Fe_2O_3 contents vs. Si/Al ratios, the full extent of the association between iron oxides and biotite can be seen (Figure 8). The calculated curve for simple mixtures of oxidized biotite and kaolinite is included in the illustration for comparison.

If the above data are mathematically processed, the points for plots of K_2O vs. Si/Al ratio and of Fe_2O_3 vs. Si/Al ratio fall within calculated boundary curves, as was illustrated by Fordham (1989). This result was taken as strong evidence that the Fe_2O_3 assigned to oxidized biotite was a structural part of the mineral,

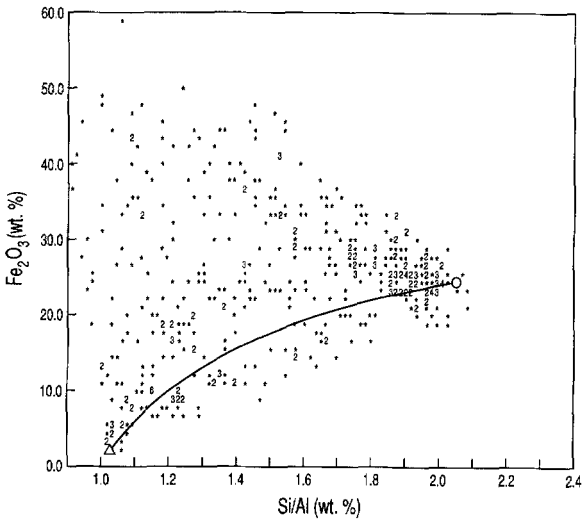

Figure 8. Microprobe analyses of biotite and its weathering products. Unprocessed data. ○——△ = mixtures of oxidized biotite ○ and kaolinite △.

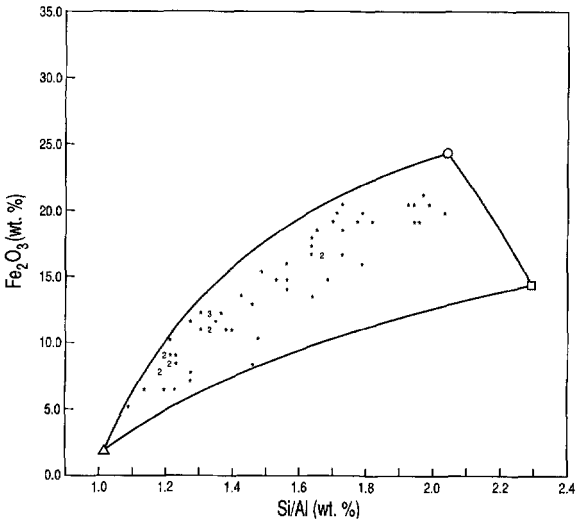

Figure 9. Microprobe analyses of weathered biotite in mottled parts of the soil profile. Unprocessed data. ○——△ = mixtures of oxidized biotite ○ and kaolinite △; ○——□ = interstratified minerals with layers of oxidized biotite ○ and of vermiculite-like mineral □; △——□ = mixtures of kaolinite △ and vermiculite-like mineral □.

or else was intimately and homogeneously (at the microprobe scale) dispersed throughout the crystal as a separate phase. The latter possibility is suggested by the work of Farmer *et al.* (1971), who showed that small domains of iron oxide are located within the interlayer region of some biotites.

Some parts of the profile were bleached or mottled as a result of reducing conditions, which gave an opportunity to measure the Fe content of biotite remnants in the absence of free iron oxides. Thin sections of such areas were generally gray in plane-polarized light, and they showed no iron oxide staining of cracks, voids, or channels. Biotite particles retained a red-brown color if they were not too decomposed, but they were commonly bleached at extremities and in exfoliations where alteration to clay minerals had occurred. Some biotite flakes even had a greenish tinge. Iron contents were generally much lower than in other parts of the profile. Plotting data from points having low Fe contents without mathematical processing, the data fall within the theoretical boundary curves (Figure 9). Displacement below the oxidized biotite-kaolinite curve is probably due to the presence of interstratified minerals. If the data are plotted after processing, the points are close to their original positions, within experimental error. This behavior confirms the validity of the Fe_2O_3 content assigned to oxidized biotite and trioctahedral illite.

Structural formulae

The large K_2O content of oxidized biotite indicates that very little K was lost during oxidation and that the interlayer charge remained relatively constant. The structural formula given below shows that octahedral occupancy is lower than in fresh biotites (Deer *et al.*, 1962) and suggests that the high interlayer charge was maintained by the expulsion of octahedral cations. Decreases in octahedral occupancy as a result of oxidation have been noted by several others (Newman and Brown, 1966; Rimsaite, 1967; Gilkes *et al.*, 1972).

The structural formula of fresh biotite from exposed boulders is also given below. It reflects the level of interlayer charge to be expected of fresh biotite; however, it cannot be compared with oxidized biotite to see if octahedral Fe was lost from the structure during oxidation, because a large part of the difference in total Fe contents of the two biotites is obviously due to substitution of Mg for Fe in oxidized biotite. Because this is an improbable result of weathering, fresh biotite from exposed boulders was not considered to be the true parent of oxidized biotite.

Oxidized biotite:

$$\underset{+1.84}{K_{1.78}}\underset{}{Na_{0.06}}(\underset{}{Si_{5.23}}\underset{}{Al_{2.65}}\underset{}{Fe^{3+}_{0.12}})\underset{-2.77,\ 8.00}{}$$

$$\cdot(\underset{}{Ti_{0.33}}\underset{}{Fe^{2+}_{0.22}}\underset{}{Fe^{3+}_{2.41}}\underset{}{Mg_{1.97}})\underset{}{O_{20}}\underset{+0.93,\ 4.93}{(OH)_4}$$

Fresh biotite:

$$\underset{+1.90}{K_{1.84}}\underset{}{Na_{0.06}}(\underset{}{Si_{5.14}}\underset{}{Al_{2.83}}\underset{}{Fe^{3+}_{0.03}})\underset{-2.86,\ 8.00}{}$$

$$\cdot(\underset{}{Ti_{0.40}}\underset{}{Fe^{2+}_{2.48}}\underset{}{Fe^{3+}_{1.63}}\underset{}{Mg_{0.75}})\underset{}{O_{20}}\underset{+0.95,\ 5.26}{(OH)_4}$$

https://doi.org/10.1346/CCMN.1990.0380210 Published online by Cambridge University Press

SUMMARY AND CONCLUSIONS

Trioctahedral illite is relatively uncommon in soils, but it has been identified by XRD in every horizon of a soil developed on granite gneiss at Mt. Crawford in South Australia. It was formed from biotite which had a high content of structural Fe that readily oxidized at a very early stage of weathering. The oxidized form constituted a large part of an intact flake before exfoliation occurred, and it retained a high K_2O content. Internal strains caused by oxidation were off-set by buckling, fracturing, and the formation of slits at cleavage planes. These physical deformations allowed entry of solutions and movement of ions, which facilitated chemical decomposition along cleavage planes in particular. Major and minor exfoliations resulted, but oxidized biotite persisted even to the stage of weathering in which the interior of small segments were subdivided repeatedly by fine exfoliation and concurrent chemical alteration to produce narrow, parallel strands separated by equally narrow layers occupied by clay-size particles.

The strands containing oxidized biotite were responsible for the retention of some optical properties of the original biotite, such as second-order interference colors, by weathered fragments. If weathered fragments were reduced to clay-size particles, residues of oxidized biotite persisted and consequently produced the XRD spacings characteristic of trioctahedral illite. The chemical composition of trioctahedral illite was taken to be the same as that derived for oxidized biotite from microprobe data. Trioctahedral illite appeared to have a relative degree of stability once it was removed from the most active weathering zone.

ACKNOWLEDGMENTS

The author is grateful to H. Rosser for his assistance with microprobe analysis, S. McClure for SEM photography and EDX analysis, R. Merry for help in collecting and impregnating samples for thin-sectioning and K. Norrish for XRF analysis and for his advice and encouragement.

REFERENCES

Bailey, S. W. (1984) X-ray powder patterns of micas: in *Micas, Reviews of Mineralogy,* **13,** S. W. Bailey, ed., Mineral. Soc. Amer., Washington, D.C., 573–584.

Bailey, S. W., Brindley, G. W., Johns, W. D., Martin, R. T., and Ross, M. (1971) Summary of national and international recommendations on clay mineral nomenclature. 1969–70 CMS Nomenclature Committee: *Clays & Clay Minerals* **19,** 129–132.

Barshad, I. and Kishk, F. M. (1968) Oxidation of ferrous iron in vermiculite and biotite alters fixation and replaceability of potassium: *Science* **162,** 127–137.

Bisdom, E. B. A. (1967) Micromorphology of a weathered granite near the Ria de Arosa (N.W. Spain): *Leidse Geol. Meded.* **37,** 33–67.

Bisdom, E. B. A., Stoops, G., Delvigne, J., Curmi, P., and Altemuller, H.-J. (1982) Micromorphology of weathering biotite and its secondary products: *Pedologie* **32,** 225–252.

Bustin, R. M. and Mathews, W. H. (1979) Selective weathering of granitic clasts: *Can. J. Earth Sci.* **16,** 215–223.

Chartres, C. J., Chivas, A. R., and Walker, P. H. (1988) The effect of aeolian successions on soil development on granitic rocks in south-eastern Australia. II. Oxygen-isotope, mineralogical and geochemical evidence for aeolian deposition: *Aust. J. Soil Res.* **26,** 17–31.

Deer, W. A., Howie, R. A., and Zussman, J. (1962) *Rock-forming Minerals, Vol. 3: Sheet Silicates:* Wiley, New York, 58–64 pp.

Farmer, V. C., Russell, J. D., McHardy, W. J., Newman, A. C. D., Ahrichs, J. L., and Rimsaite, J. Y. H. (1971) Evidence for loss of protons and octahedral iron from oxidized biotites and vermiculites: *Mineral. Mag.* **38,** 121–137.

Fordham, A. W. (1990) Treatment of microanalyses of intimately mixed products of mica weathering: *Clays & Clay Minerals* **38,** 179–186.

Fordham, A. W., Merry, R. H., and Beckmann, G. G. (1985) Site description and field observations in a study of B horizon development in duplex soils: *CSIRO Aust. Div. Soils Tech. Mem.* **14,** 12 pp.

Ghabru, S. K., Mermut, A. R., and St. Arnaud, R. J. (1987) The nature of weathered biotite in sand-sized fractions of gray luvisols (boralfs) in Saskatchewan, Canada: *Geoderma* **40,** 65–82.

Gilkes, R. J. (1973) The alteration products of potassium depleted oxybiotite: *Clays & Clay Minerals* **21,** 303–313.

Gilkes, R. J. and Suddhiprakarn, A. (1979) Biotite alteration in deeply weathered granite. 1. Morphological, mineralogical and chemical properties: *Clays & Clay Minerals* **27,** 349–360.

Gilkes, R. J. and Young, R. C. (1974) Artificial weathering of oxidized biotite: 4. The inhibitory effect of potassium on dissolution rate: *Soil Sci. Soc. Amer. Proc.* **38,** 529–532.

Gilkes, R. J., Young, R. C., and Quirk, J. P. (1972) The oxidation of octahedral iron in biotite: *Clays & Clay Minerals* **20,** 303–315.

Kapoor, B. S. (1972) Weathering of micaceous clays in some Norwegian podzols: *Clay Miner.* **9,** 383–394.

Nettleton, W. D., Nelson, R. E., and Flach, K. W. (1973) Formation of mica in surface horizons of dryland soils: *Soil Sci. Soc. Amer. Proc.* **37,** 473–478.

Newman, A. C. D. and Brown, G. (1966) Chemical changes during the alteration of micas: *Clay Miner.* **6,** 297–309.

Norrish, K. and Pickering, J. G. (1983) Clay minerals: in *Soils—An Australian Viewpoint,* Division of Soils, CSIRO/ Academic Press, London, 281–308.

Penven, M.-J., Fedoroff, N., and Robert, M. (1981) Weathering of biotites in Algeria: *Geoderma* **26,** 287–309.

Rimsaite, J. (1967) Biotite intermediate between dioctahedral and trioctahedral micas: in *Clays and Clay Minerals, Proc. 15th Natl. Conf., Pittsburgh, Pennsylvania, 1966,* S. W. Bailey, ed., Pergamon Press, New York, 375–393.

Robert, M. and Pedro, G. (1969) A study of the relationship between oxidation and degree of exfoliation in trioctahedral micas: in *Proc. Int. Clay Conf., Tokyo, 1969, Vol 1,* L. Heller, ed., Israel Prog. Sci. Transl., Jerusalem, 455–473.

Ross, G. J. and Rich, C. I. (1974) Effect of oxidation and reduction on potassium exchange of biotite: *Clays & Clay Minerals* **22,** 355–360.

Rossman, G. R. (1984) Spectroscopy of micas: in *Micas, Reviews in Mineralogy, 13,* S. W. Bailey, ed., Mineral. Soc. Amer., Washington, D.C., 145–181.

Seddoh, F. K. and Pedro, G. (1974) Characterization of different stages of transformation of biotites and chloritized biotites in granite saprolites at Morvan: *Bull. Groupe Franc. Argiles* **26,** 107–125.

Shoba, S. A. and Sokolova, T. A. (1981) Weathering products of biotite in sodpodzolic soil: *Soviet Soil Sci.* **6,** 91–97.

Soil Survey Staff (1975) *Soil Taxonomy:* U.S. Dept. Agriculture No. 436, U.S. Gov. Print. Office, Washington, D.C., 754 pp.

Środoń, J. and Eberl, D. D. (1984) Illite: in *Micas, Reviews in Mineralogy, 13,* S. W. Bailey, ed., Mineral. Soc. Amer., Washington, D.C., 495–544.

Stace, H. C. T., Hubble, D. D., Brewer, R., Northcote, K. H., Sleeman, J. R., Mulcahy, M. J., and Hallsworth, E. G. (1968) *A Handbook of Australian Soils:* Rellim, Glenside, South Australia, 435 pp.

Tarzi, J. G. and Protz, R. (1978) Characterization of morphological features of soil micas using scanning electron microscopy: *Clays & Clay Minerals* **26,** 352–360.

Tarzi, J. G. and Protz, R. (1979) Increased selectivity of naturally weathered biotites for potassium: *Soil Sci. Soc. Amer. J.* **43,** 189–191.

Walker, G. F. (1949) The decomposition of biotite in the soil: *Mineral. Mag.* **28,** 693–703.

Walker, G. F. (1950) Trioctahedral minerals in the soil-clays of north-east Scotland: *Mineral. Mag.* **29,** 72–84.

Wilson, M. J. (1966) The weathering of biotite in some Aberdeenshire soils: *Mineral. Mag.* **35,** 1080–1093.

Wilson, M. J. (1970) A study of weathering in a soil derived from a biotite-hornblende rock. 1. Weathering of biotite: *Clay Miner.* **8,** 291–303.

(Received 3 November 1988; accepted 10 May 1989; Ms. 1848)